Two-dimensional behavior of three-dimensional magnetohydrodynamic flow with a strong guiding field

Alexandros Alexakis
Laboratoire de Physique Statistique de l'Ecole Normale Supérieure, UMR CNRS 8550, 24 Rue Lhomond, FR-75006 Paris Cedex 05, France
(Received 9 September 2011; published 29 November 2011)

The magnetohydrodynamic (MHD) equations in the presence of a guiding magnetic field are investigated by means of direct numerical simulations. The basis of the investigation consists of nine runs forced at the small scales. The results demonstrate that for a large enough uniform magnetic field the large scale flow behaves as a two-dimensional (2D) (non-MHD) fluid exhibiting an inverse cascade of energy in the direction perpendicular to the magnetic field, while the small scales behave like a three-dimensional (3D) MHD fluid cascading the energy forwards. The amplitude of the inverse cascade is sensitive to the magnetic field amplitude, the domain size, the forcing mechanism, and the forcing scale. All these dependences are demonstrated by the varying parameters of the simulations. Furthermore, in the case that the system is forced anisotropically in the small parallel scales an inverse cascade in the parallel direction is observed that is feeding the 2D modes $k_\parallel = 0$.

DOI: 10.1103/PhysRevE.84.056330 PACS number(s): 47.65.−d, 95.30.Qd

I. INTRODUCTION

The existence of magnetic fields is known in many astrophysical objects, such as the interstellar medium, galaxies, accretion disks, star and planet interiors, and the solar wind [1]. In most of these systems, the magnetic fields are strong enough to play a significant dynamical role. The kinetic and magnetic Reynolds numbers involved in these astrophysical bodies are large enough so that the flows exhibit a turbulent behavior with a large continuous range of excited scales, from the largest where energy is injected, toward the finest where energy is dissipated. In many cases, strong large-scale magnetic fields are present that induce dynamic anisotropy in the small scales. Direct numerical simulations that examine in detail both large and small scale turbulent processes in astrophysical plasmas are very difficult to achieve, and only modest scale separation can be reached even with today's supercomputers. One way around this difficulty is to model the effect of the large scale field by a uniform magnetic field B_0, and thus study the small scales separately.

In the presence of a strong uniform magnetic field the evolution of the turbulent fluctuating fields can be treated within the framework of *weak turbulence theory* (WTT). In this approach the nonlinearities are treated perturbatively, resulting in a slowly varying amplitude of the linear wave modes that in this case are the Alfven waves supported by the uniform magnetic field [2,3]. However, the limit $B_0 \to \infty$ is nontrivial because different limiting procedures can lead to different results. Thus in order for the results of weak turbulence theory [2] to hold the Alfven frequency $B_0 k_\parallel$ has to be larger than the eddy-turnover frequency $u_k k_\perp$ [2,4] (where u_k is the amplitude of eddies of typical size $k_\parallel^{-1}$ in the direction of the field and $k_\perp^{-1}$ in the direction perpendicular to the field). This condition implies that the nonlinearities are small and justifies the perturbative expansion. However, for the $k_\parallel = 0$ modes that have zero frequency, this condition is never satisfied. These modes if sufficiently amplified can violate the WTT assumptions for all wave numbers since they are always involved in the triads that satisfy the resonance conditions for three-wave interactions [2,3]. Nonetheless the energy cascade in the framework of WTT theory is not based on exact resonances but rather it requires the existence of modes sufficiently close in resonance or "quasiresonances." For such resonances to exist a domain of size L (in direction of the field) sufficiently large needs to be considered, so that modes with small wave numbers in the direction of the field $k_\parallel$ that satisfy these conditions are present. More precisely WTT is valid when the following condition is met:

$$\frac{1}{\sqrt{k_\parallel L_\parallel}} \ll \frac{u_k k_\perp}{B_0 k_\parallel} \ll 1 \tag{1}$$

(see [5]), where $L_\parallel$ is the domain size in the direction of the field. The inequality on the right implies sufficiently weak nonlinearity while the inequality on the left is needed for the presence of quasiresonances. In this case WTT predicts that the energy spectrum is proportional to $k_\perp^{-2}$. On the other hand if

$$\frac{|u_k| k_\perp}{B_0 k_\parallel} \ll \frac{1}{k_\perp L_\perp} \frac{1}{\sqrt{k_\parallel L_\parallel}} \tag{2}$$

the system becomes "slaved" to the 2D modes $k_\parallel = 0$ that evolve independently [5]. Thus if the limit $B_0 \to \infty$ is taken keeping the domain size L fixed the system becomes two dimensional [5,6]. The two conditions (1) and (2) also allow the existence of an intermediate regime. Finally it is noted that for the same system different scales can have different behavior. Thus in principle strong, weak, and 2D turbulence can coexist in a flow at different scales.

Here the large B_0 limit is explored further by means of numerical simulations. Numerically, *magnetohydrodynamic* (MHD) turbulence has been investigated by various groups in the last decade [7–11]. The results of WTT were first demonstrated in [12,13] while the transition to two-dimensional dynamics has been investigated more recently in [14]. In all these investigations the flow was forced at the largest scale of the system. In this work the case where the system is forced at the small scales is explored and the possible development of an inverse cascade is examined.

An inverse energy cascade is known to exist in *two-dimensional hydrodynamic* (2D-HD) turbulence [15–17], as

a consequence of the conservation of vorticity. It results in a $k^{-5/3}$ spectrum for the large scales and a k^{-3} spectrum for the small scales. Strongly rotating flows [18–22] or flows in thin boxes [23] have been shown to have a dual cascade of energy with the large scale flow behaving like 2D with an inverse cascade while the small scales being three dimensional with a direct cascade. However, 2D MHD turbulence does not conserve the vorticity and energy is cascading to small scales. On the contrary, the square of the vector potential is cascading to larger scales [24,25]. For the system under investigation we cannot *a priori* predict if the flow under the influence of a strong magnetic field will act as a 2D-HD flow by suppressing all magnetic fluctuations and thus have an inverse cascade; or if magnetic fluctuations persist and the system will act as a 2D-MHD flow and thus not exhibit an inverse cascade of energy. It is noted that a strong magnetic field is used very often to make flows of liquid metals behaving like two-dimensional flows in experiments where an inverse cascade has been observed [26,27]. These flows however have very small magnetic Reynolds numbers and magnetic fluctuations are strongly suppressed.

II. FORMULATION AND NUMERICAL SIMULATIONS

We consider a flow of a conducting fluid inside a triple-periodic box of size $2\pi L$ in the presence of a strong guiding magnetic field B_0 in the $\hat{\mathbf{z}}$ direction. The system is forced by a mechanical force $\mathbf{f}$ and an electromotive force $\mathcal{E}$. The nondimensional MHD equations then read

$$\partial_t \mathbf{u} + \mathbf{u}\cdot\nabla\mathbf{u} = V_A \partial_z \mathbf{b} + \mathbf{b}\cdot\nabla\mathbf{b} - \nabla P + G_K^{-\frac{1}{2}}\nabla^2\mathbf{u} + \mathbf{F},$$

$$\partial_t \mathbf{b} + \mathbf{u}\cdot\nabla\mathbf{b} = V_A \partial_z \mathbf{u} + \mathbf{b}\cdot\nabla\mathbf{u} + G_M^{-\frac{1}{2}}\nabla^2\mathbf{b} + M\nabla\times\mathbf{E},$$

where $\mathbf{u}$ is the velocity field and $\mathbf{b}$ is the magnetic field. Both fields are assumed to be solenoidal $\nabla\cdot\mathbf{u} = \nabla\cdot\mathbf{b} = 0$. $\mathbf{F} = \mathbf{f}/\|\mathbf{f}\|$ is the external mechanical force normalized to unit amplitude (where $\|\cdot\|$ stands for the L_2 norm). $\mathbf{E}$ is the external electromotive force normalized so that its curl has unit amplitude $\mathbf{E} = \mathcal{E}/\|\nabla\times\mathcal{E}\|L$. The equations have been nondimensionalized using the box size L and the forcing amplitude $\|\mathbf{f}\|$. With this choice four nondimensional parameters appear. G_K is the kinetic Grashof number $G_K \equiv \|\mathbf{f}\|L^3/\nu^2$, where ν is the viscosity. G_M is the magnetic Grashof number $G_M \equiv \|\mathbf{f}\|L^3/\eta^2$, where η is the magnetic diffusivity. In all the runs performed in this work $G_K = G_M$. The amplitude of the external magnetic field relative to the forcing is controlled by the parameter $V_A \equiv B_0/\sqrt{\|\mathbf{f}\|L}$. Finally $M \equiv \|\nabla\times\mathcal{E}\|/\|\mathbf{f}\|$ expresses the ratio of the electromotive to the mechanical forcing.

A possible alternative to this nondimensionalization choice would be to use the kinetic and magnetic Reynolds numbers, typically defined as $Re \equiv \|\mathbf{u}\|L/\nu$ and $Rm \equiv \|\mathbf{u}\|L/\eta$, respectively. For our problem at hand; however, where an inverse cascade is present, it is not an attractive choice because the amplitude of the velocity is changing with time throughout the duration of the computation rendering Re a function of time.

Both forcing mechanisms used in the numerical simulations consisted of a sum of Fourier modes with wave numbers inside a spherical shell $|\mathbf{k}| = k_f$. The phases of the modes were changed randomly every time interval $\tau \sim \sqrt{L/\|\mathbf{f}\|}$. The forcing is isotropic in all runs except the last two that we discus in Sec. III E. There was no averaged helicity or cross helicity injected by the forcing by choosing $\langle\mathbf{F}\cdot\nabla\times\mathbf{F}\rangle = 0$ and $\langle\mathbf{F}\cdot\nabla\times\mathbf{E}\rangle = 0$. Since we are interested in the presence of an inverse cascade we are forcing relatively large wave numbers.

TABLE I. Table with the parameters of all runs. "I" in the last column stands for isotropic forcing. The parameters that are varied with respect to R1 are boldface.

Runs	$G_K^{\frac{1}{2}}/10^3$	V_A	$k_f L$	M_0	Isotropy
R1	5.0	5.0	8–10	0.0	I
R2	2.5	**2.0**	8–10	0.0	I
R3	2.5	**10.0**	8–10	0.0	I
R4	10.0	5.0	**4–5**	0.0	I
R5	2.5	5.0	**16–20**	0.0	I
R6	3.3	5.0	8–10	**0.4**	I
R7	2.5	5.0	8–10	**0.6**	I
R8	2.5	5.0	8–10	0.0	$\mathbf{F}(\mathbf{k}_\parallel,\mathbf{0}) = \mathbf{0}$
R9	16.0	5.0	8–10	0.0	$\mathbf{F}(\mathbf{0},\mathbf{k}_\perp) = \mathbf{0}$

The MHD equations were solved using a standard pseudospectral method and a third order in time Runge-Kutta [28,29]. The resolution used in all the runs was 512^3 grid points. In the nine different runs that were performed the amplitude of the external magnetic field, and the way the system is forced, was varied. Table I gives all the parameters of the runs.

The choice of G_K in most runs is rather conservative because it is not known beforehand what effect on the resolution requirements a change in each of the parameters has. In any case, in all runs a well resolved spectrum was observed. The last run (R9) has a large value of G_K because in this case for similar forcing amplitude with the other runs the flow is less efficient in absorbing energy because the $k_\parallel = 0$ modes are not forced. In this run also the time scale of the forcing was set to $\tau \sim (B_0 k_f)^{-1}$ to be closer in resonance with the forced Alfven modes and to improve this absorption efficiency.

The diagnostics used are based on energy spectra and energy fluxes that are now defined. If $\hat{\mathbf{u}}_\mathbf{k}$ and $\hat{\mathbf{b}}_\mathbf{k}$ are the Fourier modes of the velocity and magnetic field of wave number $\mathbf{k}$ then the two dimensional energy spectra $E_u(k_\perp,k_\parallel)$ and $E_b(k_\perp,k_\parallel)$ are defined as

$$E_u(k_\perp,k_\parallel) = \frac{1}{2}\sum |\hat{\mathbf{u}}_\mathbf{k}|^2, \quad E_b(k_\perp,k_\parallel) = \frac{1}{2}\sum |\hat{\mathbf{b}}_\mathbf{k}|^2,$$

where the sum is restricted in the wave numbers $k_\parallel \leqslant |k_z| < k_\parallel + 1$ and $k_\perp \leqslant \sqrt{k_x^2 + k_y^2} < k_\perp + 1$. The averaged energy spectra in the parallel direction are then defined as

$$\bar{E}_u(k_\perp) = \sum_{k_\parallel} E_u(k_\perp,k_\parallel), \quad \bar{E}_b(k_\perp) = \sum_{k_\parallel} E_b(k_\perp,k_\parallel).$$

The total kinetic energy E_K and magnetic energy E_M are then given by

$$E_K = \sum_{k_\perp} \bar{E}_u(k_\perp), \quad E_M = \sum_{k_\perp} \bar{E}_b(k_\perp).$$

Since the development of a direct or an inverse cascade is expected to be anisotropic, we need to define the flux of energy through an arbitrary surface in Fourier space. If $\mathbf{u}_D$ and $\mathbf{b}_D$ stand for the projection of the two fields $\mathbf{u}$,$\mathbf{b}$ to the flows whose Fourier transform contain modes only inside the Fourier domain "D," the energy flux through this domain is given by

$$\Pi_D = \int [\mathbf{u}_D\mathbf{u}\cdot\nabla\mathbf{u} - \mathbf{u}_D\mathbf{b}\cdot\nabla\mathbf{b} + \mathbf{b}_D\mathbf{u}\cdot\nabla\mathbf{b} - \mathbf{b}_D\mathbf{b}\cdot\nabla\mathbf{u}]dV.$$

See [30] for more details. In this work we will consider the flux through cylinders and planes. By $\Pi_\perp(k_\perp)$ we will refer to the flux of energy through a cylinder of radius $\sqrt{k_x^2+k_y^2}=k_\perp$ and by $\Pi_\perp(k_\parallel)$ we will refer to the flux of energy through the planes $|k_z|=k_\parallel$. Positive flux implies cascade of energy to the small scales while a negative flux implies cascade to the large scales.

III. RESULTS

A. Pilot run

The first run in Table I serves as a basic run to which all other runs are compared. For this reason this run is examined in more detail. Figure 1 shows the evolution of the kinetic and magnetic energy as a function of time. As can be seen the magnetic energy grows and saturates very fast at a relatively small amplitude. The kinetic energy, on the other hand, after an initial fast growth transitions to a slower increasing phase. Up until the end of the numerical simulation this slow growth persists. The reason for this growth is the inverse cascade of the kinetic energy that accumulates energy in the large scales.

This inverse cascade is demonstrated more clearly in Fig. 2. This figure shows the parallel and perpendicular energy flux normalized by the total energy injection rate. The perpendicular energy flux is positive for wave numbers larger than the forcing wave number (direct cascade) while for smaller wave numbers a negative constant energy flux (inverse cascade) can be seen. On the other hand, the parallel energy flux, shown by the dashed line, is small and always positive (i.e., direct).

The presence of an inverse cascade can also be indicated by looking at the energy spectra at late times. The top panel of Fig. 3 shows the kinetic energy spectrum $\bar{E}_u$ of run R1 averaged over several outputs close to the end of the simulation. It can

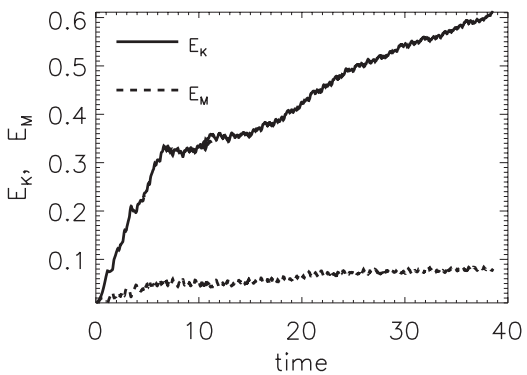

FIG. 1. Time evolution of the kinetic energy E_K (solid line) and the magnetic energy E_M (dashed line) for run R1.

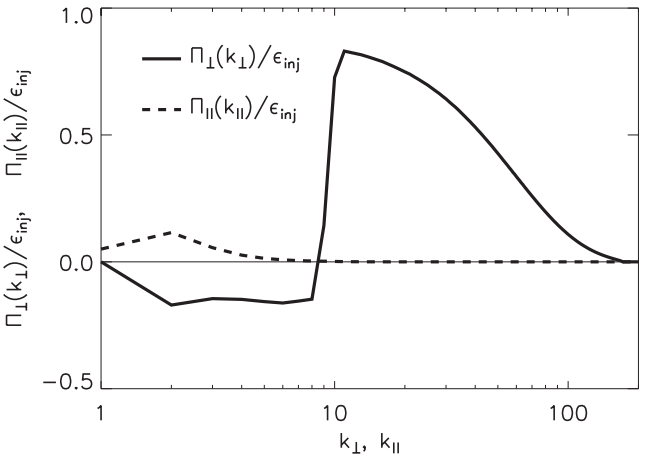

FIG. 2. The energy flux for run R1 in the perpendicular direction (solid line) and parallel direction (dashed line).

be clearly seen that most of the energy is concentrated in the large scales. The dashed line in this panel shows $E_u(0,k_\perp)$. At large scales this line is identical to the $\bar{E}_u$ spectrum, thus the

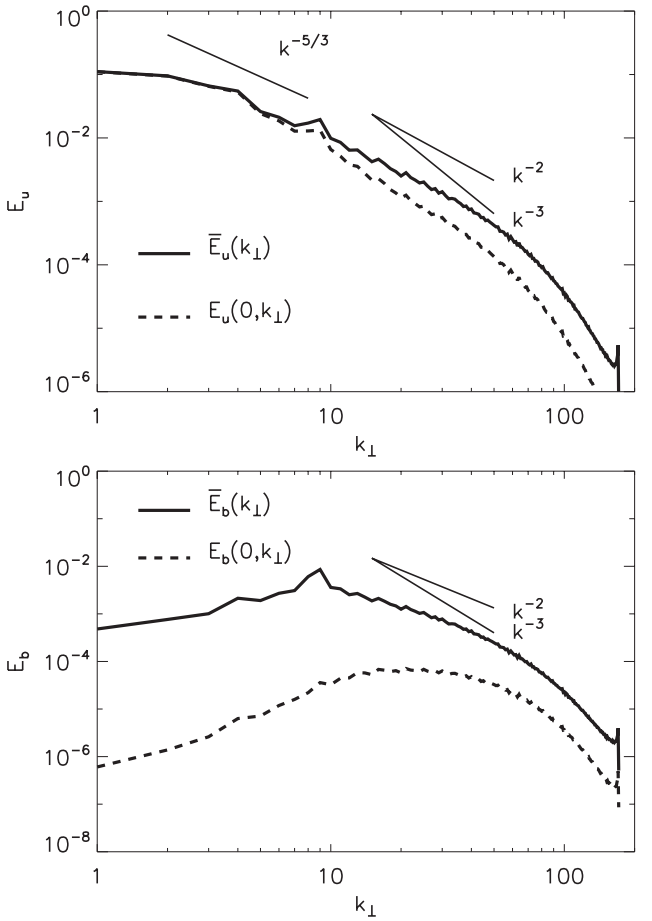

FIG. 3. Kinetic (top panel) and magnetic (bottom panel) energy spectra of run R1. The solid lines correspond to the averaged spectra $\bar{E}_u(k_\perp),\bar{E}_b(k_\perp)$ while the dashed lines indicate the zeroth component ($k_\parallel=0$) of the two-dimensional energy spectra $E_u(0,k_\perp)$ and $E_b(0,k_\perp)$. The straight lines show for reference the power-law spectra $k^{-5/3},k^{-2},k^{-3}$.

energy in these scales is mostly contained in the 2D modes $k_\parallel = 0$. This means that the flow in the large scales is almost 2D. (Here the flow is referred to as 2D in the sense that u has no dependence on the z direction and not that the u_z component is absent.) On the other hand, at the small scales $E_u(0,k_\perp)$ is significantly smaller than $\bar{E}_u$, thus the 2D modes contain only a small fraction of the energy and therefore the flow is three dimensional.

The bottom panel of Fig. 3 compares the magnetic energy spectra $E_b(0,k_\perp)$ and $\bar{E}_b$. Unlike the velocity field the magnetic field remains strongly three dimensional for all scales since $E_b(0,k_\perp) \ll \bar{E}_b$. The amplitude of the magnetic energy is much smaller than that of the kinetic energy in the large scales but of the same order in the small scales. This is essential for the presence of the 2D-inverse cascade. If the magnetic field fluctuations were strong enough in the large scales, the flow would behave as a 2D-MHD flow with a direct cascade.

The $k^{-5/3}$ scaling prediction for the 2D inverse cascade, the k^{-3} for the direct 2D cascade, and the k^{-2} prediction of WTT are shown as a reference. The observed spectra are compatible with $k^{-5/3}$ in the large scales and k^{-2} in the small scales; however, the inertial ranges in the examined flow are too small to be conclusive.

B. Guiding magnetic field strength

As a next step the dependence of the inverse cascade, observed in R1, on the amplitude of the uniform magnetic field is examined. Runs R2 and R3 have all parameters similar to run R1 but a different value of the magnetic field amplitude. The flux of energy in both directions for runs R1, R2, and R3 are compared in Fig. 4. As expected, the amplitude of the uniform magnetic field has a drastic effect on the energy flux. The top panel of this figure shows $\Pi_\perp(k_\perp)$. R2 (dashed line) that has smaller value of V_A than run R1 (solid line) has no inverse cascade and a stronger direct cascade. R3 (dashed-dot line) that has larger value of V_A has on the contrary a stronger inverse cascade and a weaker forward cascade. The bottom panel of

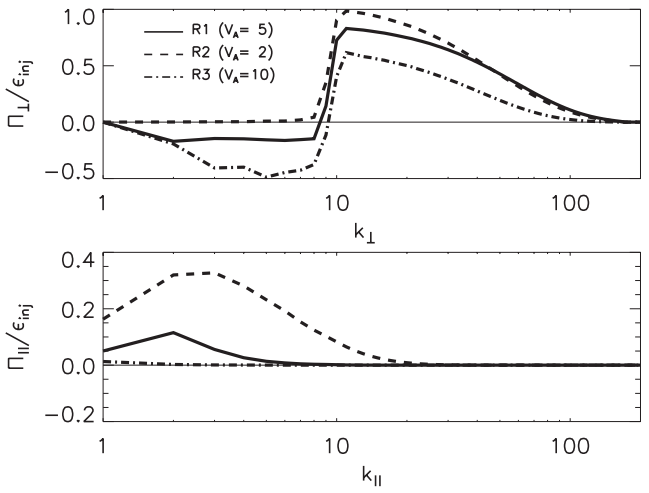

FIG. 4. Top panel: The energy flux in the perpendicular direction for R1 ($V_A = 5$, solid line), R2 ($V_A = 2$, dashed line), and R3 ($V_A = 10$, dashed-dot line). Bottom panel: The energy flux in the perpendicular direction for the same runs.

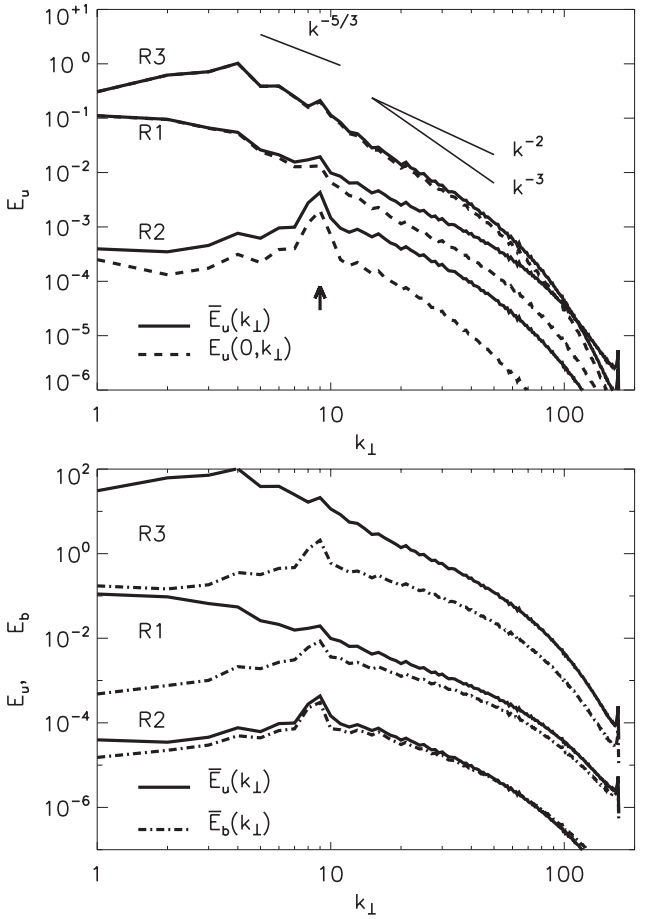

FIG. 5. Top panel: The kinetic energy spectra of $\bar{E}_u(k_\perp)$ (solid line) and $E_u(0,k_\perp)$ (dashed line) for R3, $V_A = 10$ (top lines), R1, $V_A = 5$ (middle lines), and R2, $V_A = 2$ (bottom lines). Bottom panel: The kinetic energy spectra $\bar{E}_u(k_\perp)$ (solid line) compared to the magnetic energy spectra $\bar{E}_b(k_\perp)$ (dashed line) of the same runs and with the same order. The spectra have been shifted for reasons of clarity.

Fig. 4 shows the energy flux in the parallel direction. As the magnetic field is increased the flux to large k_z is decreased. This expected since in the $V_A = \infty$ limit there is cascade only in perpendicular direction. It is noted that although V_A is larger than the root mean square of the velocity fluctuations, because the cascade moves the energy to large $k_\perp$ the ratio $u_k k_\perp / B_0 k_\parallel$ is larger than unity in the case of R2, making the cascade strong in the small scales and leading to a nonzero flux in the parallel direction.

The spectra for these runs are compared in Fig. 5. The top panel of this figure shows the kinetic energy spectra $\bar{E}_u(k_\perp)$ and $E_u(0,k_\perp)$. The spectra have been shifted for reasons of clarity. In the two runs R1 and R3 that showed an inverse cascade, energy is concentrated in the largest scales. What can also be observed is that as V_A is increased the flow comes closer to a two-dimensional flow. For R2 for which $V_A = 2$ and no inverse cascade is observed, the flow is far from two dimensional even at the largest scales.

The bottom panel panel of Fig. 5 compares the kinetic energy spectra $\bar{E}_u(k_\perp)$ (solid line) with the magnetic energy spectra $\bar{E}_b(k_\perp)$ (dashed line). As the uniform magnetic field is increased the magnetic fluctuations are decreased compared

to the velocity fluctuations. Note that for R3 the magnetic fluctuations are almost negligible in all scales while for R2 the two fluctuating fields are in equipartition. A possible interpretation for this behavior is the following. Since in these runs there is no forcing for the magnetic field the magnetic fluctuations can be generated only by the stretching of field lines of the uniform component or by a dynamo mechanism. However, since the flow comes close to a 2D flow as V_A is increased, neither of these mechanisms is possible. The dynamo mechanism however could depend on the magnetic Reynolds number that for these runs is relatively small.

C. Forcing scale

The second parameter we examine is the forcing scale $k_f L$. This parameter is important because it controls the number of modes that satisfy the quasiresonance conditions (1) and (2). The energy flux of runs R4 with $4 < k_f \leqslant 5$ and R5 with $16 < k_f \leqslant 20$ are compared to the energy flux of R1 with $8 < k_f \leqslant 10$ in Fig. 6. The top panel again shows the energy flux in the perpendicular direction while the bottom panel shows the energy flux in the parallel direction.

All flows show an inverse cascade in the perpendicular direction. R4 has an inverse cascade of the same amplitude with R1 while R5 that is forced in smaller scales has a weaker inverse cascade. This is somehow expected since when the forcing is in smaller scales the system is closer in violating condition (2) for 2D behavior. Note also that R4 has a larger flux in the parallel direction.

The spectra for these runs are shown in Fig. 7. All runs have most of the kinetic energy concentrated in the large scales that behave like 2D-hydrodynamic flows: $\bar{E}_u(k_\perp) \simeq E_u(0,k_\perp)$ (top panel) and $\bar{E}_u(k_\perp) \gg \bar{E}_b(k_\perp)$ (bottom panel). The scales smaller than the forcing scale on the other hand behave like 3D-MHD flows with $\bar{E}_u(k_\perp) > E_u(0,k_\perp)$ and $\bar{E}_u(k_\perp) \simeq \bar{E}_b(k_\perp)$.

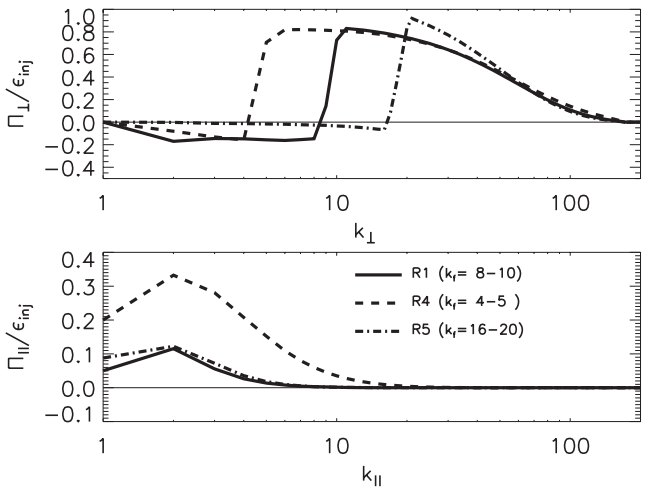

FIG. 6. Top panel: The energy flux in the perpendicular direction for R1 ($8 < k_f \leqslant 10$, solid line), R4 ($4 < k_k \leqslant 5$, dashed line), and R5 ($16 < k_f \leqslant 20$, dashed-dot line). Bottom panel: The energy flux in the perpendicular direction for the same runs.

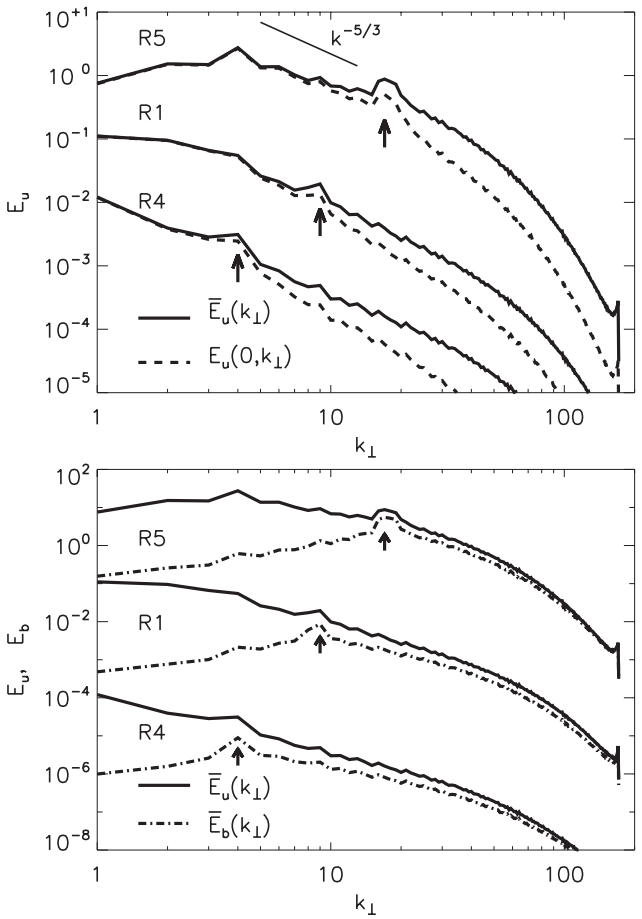

FIG. 7. Top panel: The kinetic energy spectra of $\bar{E}_u(k_\perp)$ (solid line) and $E_u(0,k_\perp)$ (dashed line) for R5 (top lines), R1 (middle lines), and R4 (bottom lines). Bottom panel: The kinetic energy spectra $\bar{E}_u(k_\perp)$ (solid line) compared to the magnetic energy spectra $\bar{E}_b(k_\perp)$ (dashed line) of the same runs and with the same order. The spectra have been shifted for reasons of clarity. The arrows indicate the location of the forcing.

D. Mechanical and electromotive forcing

The inverse cascade observed in some of the discussed runs is a property of 2D hydrodynamic turbulence that is not present in 2D-MHD turbulence. The reason it appears in the previous runs is that the amplitude of the magnetic field fluctuations in the large scales remains weak. This effect could possibly be destroyed by a large scale dynamo at larger magnetic Reynolds numbers. Leaving this possibility open the existence of the inverse cascade is investigated when magnetic field fluctuations are amplified by an electromotive force. This is examined in runs R6 and R7 where both the mechanical and the electromotive force are present.

Figure 8 shows the energy flux for runs R6 with $M = 0.4$ and R7 with $M = 0.6$ compared with R1 for which $M = 0$. The introduction of the electromotive force ($M \neq 0$) destroys the inverse cascade in the perpendicular direction (top panel), while little change is observed in the parallel direction (bottom panel). This change indicates that the system transitions from an hydrodynamic 2D state to a forward cascading MHD state.

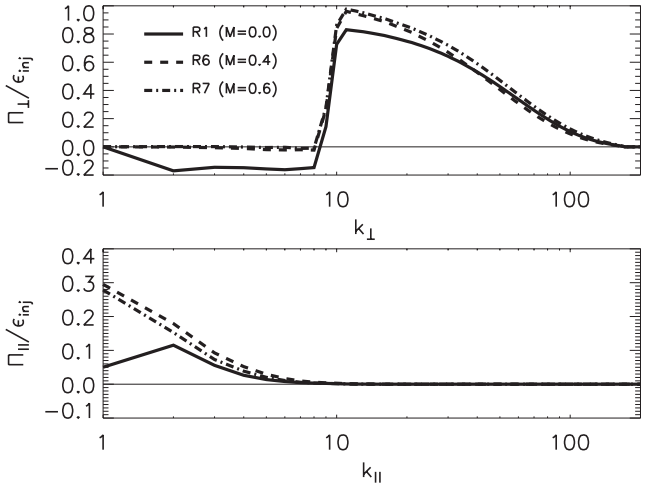

FIG. 8. Top panel: The energy flux in the perpendicular direction for R1 ($M = 0$, solid line), R6 ($M = 0.4$, dashed line), and R7 ($M = 0.6$, dashed-dot line). Bottom panel: The energy flux in the perpendicular direction for the same runs.

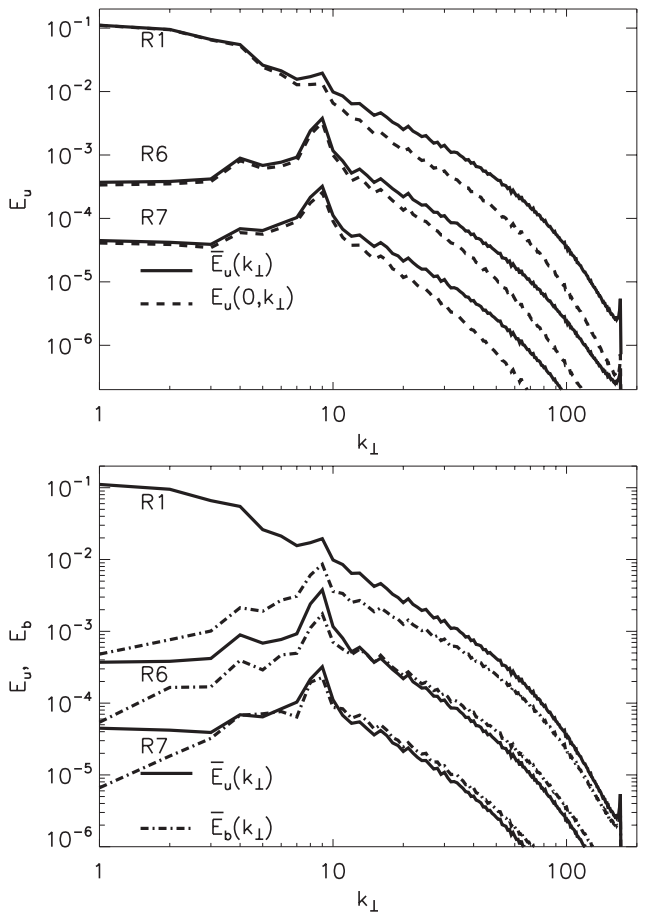

FIG. 9. Top panel: The kinetic energy spectra of $\bar{E}_u(k_\perp)$ (solid line) and $E_u(0,k_\perp)$ (dashed line) for R1, $M = 0$ (top lines), R6, $M = 0.4$ (middle lines), and R7 $M = 0.6$ (bottom lines). Bottom panel: The kinetic energy spectra $\bar{E}_u(k_\perp)$ (solid line) compared to the magnetic energy spectra $\bar{E}_b(k_\perp)$ (dashed line) of the same runs and with the same order. The spectra have been shifted for reasons of clarity.

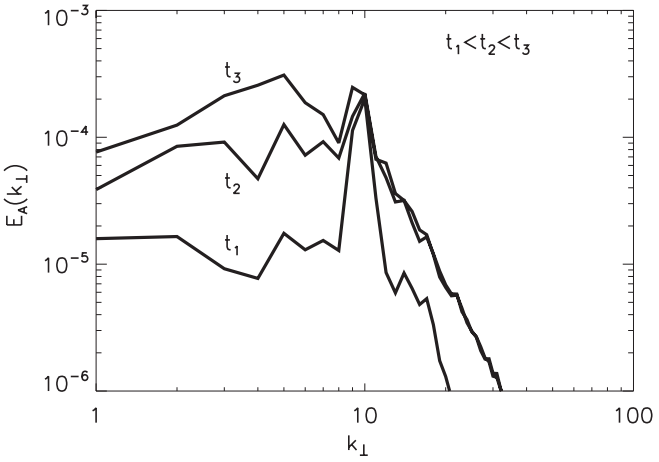

FIG. 10. The vector potential spectrum $\bar{E}_A$ for three different times.

This is further confirmed by looking at the energy spectra in Fig. 9. The top panel compares again the kinetic energy spectra $\bar{E}_u$ and $E_u(0,k_\perp)$. The excess of kinetic energy that is present in the large scales for run R1 is absent in runs R6 and R7, verifying further the absence of the inverse cascade in the presence of an electromotive force. Note that in all runs the large scales are still two-dimensional $\bar{E}_u \simeq E(0,k_\perp)$ (top panel) but the condition $\bar{E}_u(k_\perp) \gg \bar{E}_b(k_\perp)$ is true only for R1 (bottom panel). This indicates that the absence of the inverse cascades for runs R6 and R7 is not because the flow stops behaving like a 2D flow, but rather because it starts behaving like a 2D-MHD flow.

In 2D-MHD flows however there is an inverse cascade of the square of the vector potential that is a conserved quantity. If the flow in runs R6 and R7 behave like a 2D-MHD flow in the large scales such a cascade should be observed. However a flux for the squared vector potential in three dimensions cannot be uniquely defined since it is not a conserved quantity. Nonetheless, we plot the vector potential spectra for three different times from run R7 in Fig. 10. The vector potential $\mathbf{a}$ is defined so that $\mathbf{b} = \nabla \times \mathbf{a}$ and $\nabla \cdot \mathbf{a} = 0$. Its spectrum is then defined as

$$\bar{E}_A(k_\perp) = \frac{1}{2} \sum |\hat{\mathbf{a}}_\mathbf{k}|^2, \tag{3}$$

where the sum is restricted in the wave numbers $k_\perp \leqslant \sqrt{k_x^2 + k_y^2} < k_\perp + 1$ and $\hat{\mathbf{a}}_\mathbf{k}$ is the Fourier transform of $\mathbf{a}$. It can be seen that as time progresses the vector potential is increasing in the large scales. It is noted that a quasiconservation of the square of the vector potential has been observed in [31,32] for three-dimensional ideal reduced MHD.

E. Isotropic and anisotropic forcing

The last parameter that we vary is the isotropy of the forcing. Unlike the previously examined runs for which all Fourier modes within a spherical shell are uniformly forced in runs R8 and R9 the modes $k_\parallel = 0$ and $k_\perp = 0$, respectably, are forced preferentially. In particular, the amplitude of a Fourier mode $\mathbf{F_k}$ of the forcing inside the chosen spherical

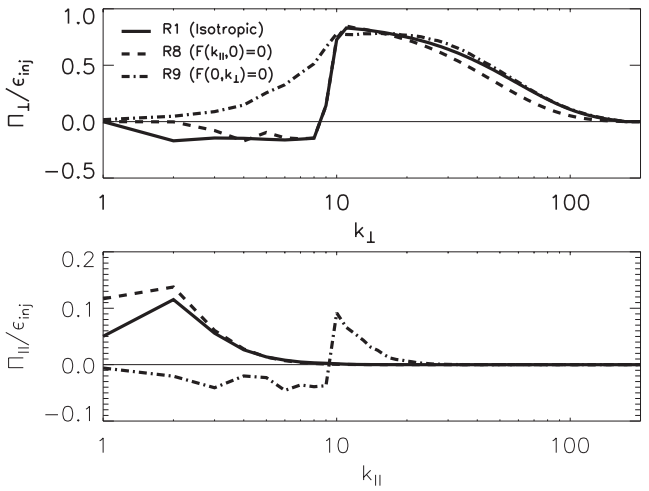

FIG. 11. Top panel: The energy flux in the perpendicular direction for R1 (solid line), R8 (dashed line), and R9 (dashed-dot line). Bottom panel: The energy flux in the perpendicular direction for the same runs.

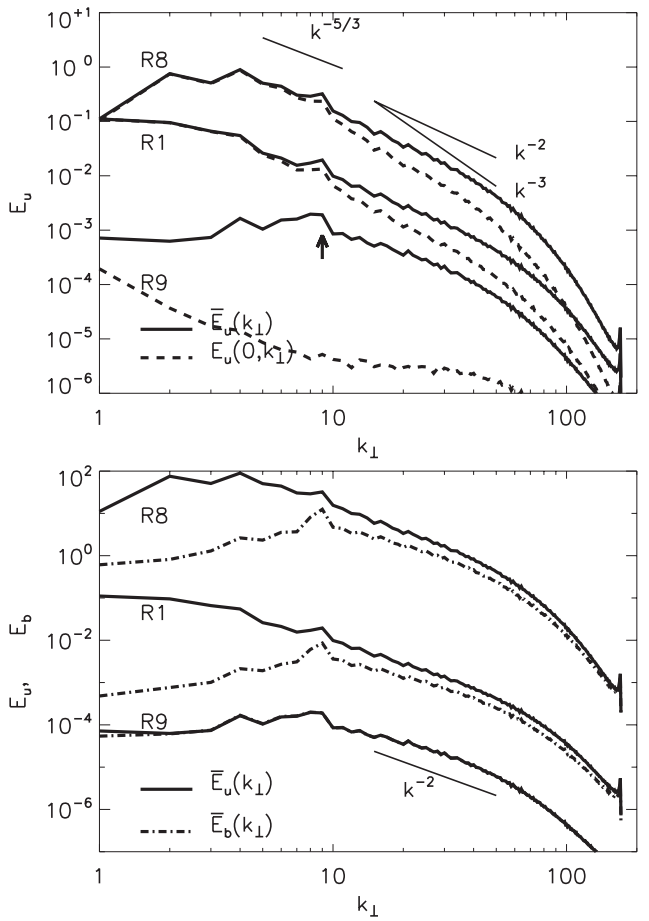

FIG. 12. Top panel: The kinetic energy spectra of $\bar{E}_u(k_\perp)$ (solid line) and $E_u(0,k_\perp)$ (dashed line) for R8 (top lines), R1 (middle lines), and R9 (bottom lines). Bottom panel: The kinetic energy spectra $\bar{E}_u(k_\perp)$ (solid line) compared to the magnetic energy spectra $\bar{E}_b(k_\perp)$ (dashed line) of the same runs and with the same order. The spectra have been shifted for reasons of clarity.

shell was proportional to

$$\text{R8}: \ |\mathbf{F_k}| \propto \frac{k_x^2 + k_y^2}{k^2}, \quad \text{R9}: \ |\mathbf{F_k}| \propto \frac{k_z^2}{k^2}, \tag{4}$$

where $k^2 = k_x^2 + k_y^2 + k_z^2$. Thus in run R8 the 2D modes ($k_z = 0$) are forced preferentially while in run R9 these 2D modes are not forced at all and most forcing is at the high k_z modes.

The energy flux for these runs is shown in Fig. 11. The energy flux of runs R1 and R8 are very close for both directions. The reason for the slightly smaller flux of R8 at the largest scales is because R8 was evolved for a shorter time than R1. R9 however has no inverse cascade in the perpendicular direction (top panel). This is not surprising since for this run the 2D modes are not forced at all. In the parallel direction there is also a drastic change. R9 shows an inverse cascade from the large k_z wave numbers to the 2D $k_z = 0$ modes. It is noted that the flux toward the large parallel scales was strongly fluctuating taking both positive and negative values. Only after averaging several files the result shown in Fig. 11 was obtained.

The spectra for these runs are shown in Fig. 12. Again not a lot of difference can be seen between run R1 and R8. Both are close to two dimensional in the large scales and three dimensional in the small scales (top panel), and both have weak magnetic energy in the large scales but are close to equipartition in the small scales (bottom panel). R9 on the other hand is three dimensional for all scales and kinetic and magnetic energy are almost identically equal at all scales. This last remark indicates that Alfven waves (for which $\mathbf{u} = \pm\mathbf{b}$) dominate the turbulence.

IV. SUMMARY AND DISCUSSION

In this work we have shown that under certain conditions an MHD flow in the presence of a strong magnetic field can behave like a two-dimensional flow in the large scales while like a three dimensional (possibly weak turbulence) in the small scales, much like strongly rotating fluids. In the large scales it was found that the magnetic fluctuations were suppressed and a 2D inverse cascade of energy developed with energy accumulating in the large scales.

This inverse cascade however is sensitive to various parameters. If the uniform magnetic field amplitude is decreased sufficiently, or if the domain size is increased (or equivalently the forcing scale is decreased) the flow recovers its 3D behavior and cascades the energy forward. Furthermore, in the case that an electromotive force is introduced the flow remains 2D but a direct energy cascade is observed. Finally, absence of an inverse cascade in the perpendicular direction is also observed when the system is forced only in the large $k_\parallel$ modes. In this case an inverse cascade in the direction parallel to the magnetic field exists.

The sensitivity of the inverse cascade to the strength of the magnetic field and the box size only reflects the validity of the condition (2) for two dimensionalization of the flow. For the inverse cascade to be present the system has to be in the 2D regime defined by inequality (2). If it is violated the systems ceases to behave like 2D flow but rather like weak or strong turbulence with a forward cascade of energy.

The absence of the cascade in the presence of an electromotive force ($M > 0$) is due to a different reason. Although condition (2) is satisfied the electromotive force results in a nonnegligible magnetic energy in the forcing scales and the system behaved as a 2D-MHD flow. As discussed in Sec. I 2D-MHD does not conserve vorticity and thus it does not exhibit an inverse cascade of energy but rather an inverse cascade of the squared vector potential. Accordingly, in the runs R6 and R7 the energy cascades forward while an inverse cascade of the squared vector potential is observed.

The transition from a forward to a backward energy cascading system is expected to happen when the magnetic energy is sufficiently strong so that the vorticity conservation is violated. However the exact value of the magnetic energy for which this transition occurs can depend on the choice of forcing, and the scale of the magnetic field. In the present case where it is the amplitude of the electromotive force that is specified, the resulting amplitude of the magnetic field can depend on the value of the magnetic Reynolds number R_M and the applied field strength V_A. A study that determines the properties of this transition is beyond the scope of this work and is left for future work.

Finally, in the case of anisotropic forcing for which the 2D modes were not forced showed absence of an inverse cascade. The system instead was dominated by Alfven waves whose interactions was cascading energy to large $k_\perp$. This confirms previous investigations [12,13] that showed that weak turbulence is observed in numerical simulations for which the 2D modes were not forced. The inverse cascade in the parallel direction however still lacks a theoretical understanding. Phenomenological estimates for the cascade in the parallel direction have been derived before in the literature [33] but were assumed then in the forward direction (towards large $k_\parallel$). More recently, during the revision of the present paper an estimate for the cascade process in the presence or absence of the forcing of the 2D modes has also been proposed [34]. Such estimates however need to be verified by future numerical simulations and experiments.

All the simulations presented here that exhibited an inverse cascade were stopped before the largest scale of the system was reached due the computational cost. If the runs were continued for a longer time as the energy and the perpendicular wave number are increased, it is possible that a point will be reached that the strength of the magnetic field will not be sufficient to stop three-dimensional instabilities from breaking the two-dimensional constrain. Such a transition point is expected to appear when the eddy turn over frequency $u_k k_\perp$ becomes larger than the smallest Alfven frequency $B_0 k_\parallel$ of a 3D perturbation (i.e., $k_\parallel \neq 0$). In the inertia range of the inverse 2D cascade where the $k_\perp^{-5/3}$ scaling is expected the eddy turnover frequency is decreasing as larger scales are reached. On the contrary, the smallest Alfven frequency $B_0 k_\parallel \sim B_0/L_\parallel$ depends only on the box size. Thus the ratio $u_k k_\perp / B_0 k_\parallel$ will decrease as the cascade proceeds and it is not expected that such a transition point will exist in the inertial range, instead as the cascade proceeds the flow will come closer to a 2D flow. However, since there is no large-scale damping mechanism to dissipate the energy when the largest scale of the system is reached, the energy would pile up in this scale. In this case the eddy turnover frequency will increase and eventually the criterion (2) for two dimensionality will be violated. Then energy could possibly return to the small scales as weak or strong turbulence. Similar scenario for the fate of the inverse cascade of rotating turbulence has been proposed in [35].

The sensitivity of the results on the domain size and type of forcing poses a number of questions on the ability to model the effect of large scale fields on small scales by a uniform field B_0. Even if large enough magnetic fields are generated (by an alpha-dynamo mechanism for example) such that the inequality on the left of (1) is satisfied it will still remain unknown whether the flow will behave in a weak turbulence manner or like a quasi-2D-MHD (or HD) flow. Further numerical and theoretical studies would then be helpful to clarify this issue.

ACKNOWLEDGMENTS

Computations were carried out on the CEMAG computing center on the CINES computing center, and their support is greatly acknowledged. The author would also like to thank the participants of the "Dynamics and turbulent transport in plasmas and conducting fluids" workshop in Les Houches, France 2011 for their useful discussions and suggestions.

[1] Ya. B. Zeldovich, A. A. Ruzmaikin, and A. A. Sokoloff, *Magnetic Fields in Astrophysics* (Gordon and Breach, New York, 1990).
[2] S. Galtier, S. V. Nazarenko, A. C. Newell, and A. Pouquet, J. Plasma Phys. **13**, 447 (2000).
[3] S. V. Nazarenko, *Wave Turbulence* (Springer, Berlin, 2011).
[4] P. Goldreich and S. Sridhar, Astrophys. J. **438**, 763 (1995).
[5] S. V. Nazarenko, New J. Phys. **9**, 307 (2007).
[6] D. Montgomery and L. Turner, Phys. Fluids **24**, 825 (1981).
[7] J. Cho and E. T. Vishniac, Astrophys. J. **539**, 273 (2000).
[8] J. Maron and P. Goldreich, Astrophys. J. **554**, 1175 (2001).
[9] J. Mason, F. Cattaneo, and S. Boldyrev, Phys. Rev. E **77**, 036403 (2008).
[10] A. Beresnyak and A. Lazarian, Astrophys. J. **702**, 1190 (2009).
[11] A. Beresnyak, Phys. Rev. Lett. **106**, 075001 (2011).
[12] J. C. Perez and S. Boldyrev, Astrophys. J. **672**, L61 (2007).
[13] B. Bigot, S. Galtier, and H. Politano, Phys. Rev. Lett. **100**, 074502 (2008).
[14] B. Bigot and S. Galtier, Phys. Rev. E **83**, 026405 (2011).
[15] R. H. Kraichnan, Phys. Fluids **10**, 1417 (1967).
[16] C. E. Leith, Phys. Fluids **11**, 671 (1968).
[17] G. K. Batchelor, Phys. Fluids **12**, 233 (1969).
[18] L. Jacquin, O. Leuchter, C. Cambon, and J. Mathieu, J. Fluid Mech. **220**, 1 (1990).
[19] C. N. Baroud, B. B. Plapp, H. L. Swinney, and Z.-S. She, Phys. Fluids **15**, 2091 (2003).

[20] P. D. Mininni and A. Pouquet, Phys. Rev. E **79**, 026304 (2009).
[21] P. D. Mininni and A. Pouquet, Phys. Fluids **22**, 035105 (2010).
[22] M. Thiele and W. Müller, J. Fluid Mech. **637**, 425 (2009).
[23] Antonio Celani, S. Musacchio, and D. Vincenzi, Phys. Rev. Lett. **104**, 184506 (2010).
[24] D. Fyfe and D. Montgomery, J. Plasma Phys. **16**, 181 (1976).
[25] A. Pouquet, J. Fluid Mech. **88**, 1 (1978).
[26] J. Sommeria, J. Fluid Mech. **170**, 138 (1986).
[27] P. Tabeling, B. Perrin, and S. Fauve, Europhys. Lett. **3**, 459 (1987).
[28] D. O. Gomez, P. D. Mininni, and P. Dmitruk, Adv. Space Res. **35**, 899 (2005).
[29] D. O. Gomez, P. D. Mininni, and P. Dmitruk, Phys. Scr., T **116**, 123 (2005).
[30] A. Alexakis, B. Bigot, H. Politano, and S. Galtier, Phys. Rev. E **76**, 056313 (2007).
[31] S. Servidio and V. Carbone, Phys. Rev. Lett. **95**, 045001 (2005).
[32] P. Dmitruk, P. D. Mininni, A. Pouquet, S. Servidio, and W. H. Matthaeus, Phys. Rev. E **83**, 066318 (2011).
[33] A. Alexakis, Astrophys. Lett. **667**, 93 (2007).
[34] A. A. Schekochihin, S. V. Nazarenko, and T. A. Yousef, e-print arXiv:1110.6682v1.
[35] S. V. Nazarenko and A. A. Schekochihin, J. Fluid Mech. **677**, 134 (2011).